Shallow donor and deep DX-like center in InAlN layers nearly lattice-matched to GaN

Marcel A. Py,* Lorenzo Lugani, Yoshitaka Taniyasu,† Jean-François Carlin, and Nicolas Grandjean
Institute of Condensed Matter Physics (ICMP), Ecole Polytechnique Fédérale de Lausanne (EPFL), CH-1015 Lausanne, Switzerland
(Received 9 May 2014; published 25 September 2014)

Nonintentionally doped 200-nm-thick $In_{0.16}Al_{0.84}N/n^+$-GaN samples were grown by metal-organic vapor phase epitaxy and used for the electrical characterization of InAlN. In the temperature range 180–400 K, the forward current of Schottky diodes is dominated by a tunneling mechanism below 1.2 V. Capacitance and conductance-temperature characteristics were measured at 1 MHz in the 90–400 K range and at various voltages. The conductance vs temperature reveals two peaks D_1 and D_2, which are attributed to bulk states in InAlN. Their characterization by admittance spectroscopy gives thermal activation energies of ≈68 meV and 290 meV, and thermal capture cross section of 9.7×10^{-17} cm^2 and $\approx 6.2 \times 10^{-15}$ cm^2, respectively. The same levels are also revealed by extracting the temperature dependence of the carrier density in the neutral region of InAlN from *I-V-T* characteristics on the Schottky diode. A partial carrier freeze out is demonstrated and discussed in the framework of an existing theory for DX centers. The use of this approach is supported by the evidence of persistent photoconductivity effects, which strongly indicate the presence of DX centers in our material. It results that each donor in InAlN would exist in two distinct lattice configurations, a substitutional one (D_1, hydrogenic state) and a lattice-distorted one (D_2, DX state). From secondary ion mass spectrometry data, theoretical grounds, and previous experimental evidence in the $Al_xGa_{1-x}N$ system, oxygen is the most probable candidate for such an unintentional dopant.

DOI: 10.1103/PhysRevB.90.115208 PACS number(s): 71.55.Eq, 73.61.Ey

I. INTRODUCTION

$In_xAl_{1-x}N$ ($x \approx 0.17$) nearly lattice-matched to GaN has a great potential to realize strain-free InAlN/GaN heterostructures for photonic and electronic applications [1]. Indeed, high reflectivity InAlN/GaN distributed Bragg reflector [2] and InAlN electron blocking layer in LEDs [3] have been demonstrated. High drain current (above 2 A/mm) InAlN/AlN/GaN high electron mobility transistors (HEMTs) have been realized [4]. They can be operated up to 900 °C for 50 hours, indicating their extreme robustness [5]. In the field of high-frequency applications, Yue *et al.* [6] achieved record current cutoff frequency f_t of 370 GHz in 30 nm gate InAlGaN/AlN/GaN HEMTs. InAlN was also used for solar-blind UV photodiodes [7]. Thick InAlN layers (>50 nm) find applications as cladding layers in edge emitting lasers [8] and wave guides.

A remaining problem with the $In_xAl_{1-x}N$ material is its fairly high *n*-type residual concentration, which lies typically around 2×10^{18} cm^{-3} in 100-nm-thick InAlN layers grown by metalorganic vapor phase epitaxy (MOVPE). The best reported value of residual doping was 6.4×10^{17} cm^{-3} in a 106-nm-thick $In_xAl_{1-x}N$ layer [9]. For thick layers, we observe that the residual doping sharply increases above 200 nm and reaches the 10^{19} cm^{-3} range for layers thicker than 400 nm. Secondary ion mass spectrometry [10–12] (SIMS) indicates that oxygen is a dominant impurity with concentrations $2–10 \times 10^{18}$ cm^{-3} but its role in the electrical properties of InAlN has not been established so far. To our knowledge, there are only few reports on the conductivity or Hall characterization of InAlN layers, even at room temperature. The reason for this lack of data comes from the fact that InAlN layers are usually grown on a GaN buffer, thus not suitable for Hall measurements because the highly conducting polarization-induced two-dimensional electron gas (2DEG) at the heterointerface masks completely the contribution from the InAlN top layer. Using semi-insulating GaAs substrates, Abernathy *et al.* [13] found that the room-temperature electron concentration of InAlN grown by metalorganic molecular beam epitaxy (MBE) decreased sharply as the AlN content was increased, from 1×10^{19} cm^{-3} at an Al content of 0.3 to less than 1×10^{16} cm^{-3} at an Al content of 0.6. A similar trend was reported by Yeh *et al.* [14] in InAlN films grown by pulsed-dc sputtering on AlN/glass, with an electron concentration of about 10^{16} cm^{-3} at an Al content of 0.49. For InAlN grown by plasma-assisted (PA)-MBE on sapphire, Lukitsch *et al.* [15] found high resistivities of $\approx 1 \times 10^4$ and 1×10^8 Ω cm for Al contents of 0.66 and 0.72, respectively. King *et al.* [16] reported also insulating behavior of Al-rich InAlN alloys grown by PA-MBE on AlN/sapphire. The role of oxygen was not discussed in these papers but the low electron density that was reported contrasts with the high oxygen concentration. These facts are difficult to reconcile with a pure shallow donor behavior of oxygen, except if there is a high concentration of compensating acceptors. Another possibility is the presence of DX centers [17,18] associated with oxygen. Indeed, it was theoretically predicted in AlN [19–24] and in Al-rich AlGaN [19–23] that oxygen forms a DX center. Considering the large band-gap value (≈4.5 eV) of InAlN nearly lattice matched to GaN, DX centers might also form in this compound. This eventuality was briefly mentioned by Chung *et al.* [11]. It follows that the investigation of deep levels in InAlN is necessary to understand the role of oxygen and other impurities in this alloy. Unfortunately, only a few results can be found in the literature. Johnstone *et al.* [25] reported two traps, one detected by deep level transient spectroscopy (DLTS), the other by admittance spectroscopy. Chen *et al.* [26] found three deep levels by capacitance DLTS whereas Chikhaoui *et al.* [27] detected one deep level by

*Corresponding author: marcel.py@epfl.ch
†Permanent address: NTT Basic Research Laboratories, NTT Corporation, 3-1, Morinosato Wakamiya, Atsugi 243-0198, Japan.

current DLTS. However, there is no consensus between the various reported signatures of the deep levels, and no attempts were done to assign them. Our own DLTS investigations of InAlN reveal the presence of two dominant broad DLTS peaks in the temperature range 150–400 K, with nonexponential behavior of the thermal emission transients, a potential source of errors in the evaluation of thermal activation energies and cross sections when standard analysis is used. In samples with nonexponential transients, it is preferable to use the admittance spectroscopy technique [28], which probes the thermal emission rate at one location point of the space-charge region upon the application of a small ac modulating signal.

The objective of this work is to characterize deep levels and the nature of the parasitic residual doping in $In_{0.16}Al_{0.84}N$ by admittance spectroscopy and current-voltage-temperature measurements on Schottky diodes. We found two levels—a shallow and a deep level—which are also evidenced in the plot of the carrier density versus inverse temperature. The two levels are probably not independent and an analogy is found with DX centers in Si-doped AlGaAs. The presence of DX centers in $In_{0.16}Al_{0.84}N$ is supported by persistent photoconductivity (PPC) experiments. From SIMS and theoretical grounds, oxygen is a likely candidate for such a dopant existing either in a substitutional nitrogen site or in a lattice-distorted configuration. Furthermore, the capacitance-voltage-temperature characteristics reflect the main features of a semiconductor with a deep level and partial carrier freeze out at low temperatures [29]. This freeze out is also evidenced from the saturation current extracted from the current-voltage-temperature characteristics of the Schottky diodes in the thermionic-field emission regime.

II. EXPERIMENTAL DETAILS AND BASIC CHARACTERIZATION

Nearly lattice-matched InAlN/GaN heterostructures were grown on 2-in. *c*-plane sapphire substrates in an Aixtron 200/4 RF-S MOVPE system [2,12]. As we target capacitive characterization, the use of layers thicker than the depletion width avoids spurious effects from surface states at the InAlN/GaN interface, and from the 2DEG. We therefore decided to investigate 200-nm-thick layers, keeping in mind that beyond this limit the residual doping sharply rises. The 200-nm-thick InAlN layers were unintentionally doped while the 2-μm-thick GaN underlying layer was Si doped. InAlN was deposited at 860 °C under N_2 at a pressure of 75 mbar. Sources were trimethylaluminum (TMA), trimethylindium (TMI), trimethylgallium (TMG), triethylgallium (TEG), and ammonia (NH_3). In this study, we prepared two samples, in which the InAlN layers were grown at different growth rates of 118 nm/hr (sample A) and 72 nm/hr (sample B), by changing only the TMA flow rate. Silane (SiH_4) was used for *n*-type doping in the GaN underlying layer, grown using a H_2 carrier gas. For PPC experiments, a HEMT heterostructure was also grown on sapphire. It is composed of a semi-insulating GaN buffer over which was deposited a barrier stack consisting of a 1-nm AlN spacer followed by a 4-nm InAlN layer. The insertion of a thin AlN spacer is widely used for improving the mobility in the 2DEG, thanks to a reduction of alloy and interface roughness scattering.

The structural characterizations of the samples were performed by high-resolution x-ray diffraction (HXRD) measurements [12], which confirmed that the InAlN layers were single phase and coherently grown on the GaN underlying layer. The In composition of InAlN was estimated to be 16.1% for the high-growth-rate sample (A) and 15.4% for the low-growth-rate sample (B). The InAlN layers are both under slight tensile strain since the lattice-matched condition of InAlN on GaN is obtained for an In composition close to 17%.

The surface morphologies of the InAlN layers were observed by atomic force microscopy (AFM). The surfaces showed hillocks together with V pits [12,30]. The height and width of the hillocks were approximately 2 nm and 100–150 nm, respectively, for both samples. The pit density was 3.5×10^9 cm^{-2} for sample A and 8×10^8 cm^{-2} for sample B.

The unintentional doping profile in InAlN layers was obtained by electrochemical *C-V* measurements (EC-V, no etching mode) with a Dage profiler CVP21 system, which operates in the kHz frequency range. The InAlN layers turned out to be *n* type with a net donor concentration $N_D - N_A$ of 2.4×10^{18} cm^{-3}, which seems to increase near the surface. The residual donor originates probably from oxygen, as this value of $N_D - N_A$ is close to the bulk oxygen concentration determined by SIMS profiling in another Si-doped 100-nm InAlN layer grown in the same reactor [12]. An oxygen concentration [O] of 3×10^{18} cm^{-3} and a carbon concentration [C] of 1.5×10^{18} cm^{-3} was measured close to the InAlN/GaN interface. [O] and [C] gradually increase from the interface to the surface, to reach about 1×10^{19} cm^{-3} and 3×10^{18} cm^{-3}, respectively, at a depth of 20 nm. Regarding the oxygen content, it is not known if this increase near the surface is due to an increased incorporation at the surface pits or to a partial surface oxidation and contamination arising after the growth [12]. Alternatively, part of the oxygen atoms could segregate during the growth and form an accumulation layer at the surface, as found by SIMS in Al-rich AlGaAs layers [31,32].

In order to gain a deeper understanding of these parasitic donors, we processed Schottky diodes for capacitive investigations, in particular by admittance spectroscopy. To realize such devices, mesa isolation was performed with dry etching in chloride-based plasma. For the annular Ohmic contacts, a Ti/Al/Ti/Au stack (40/150/40/40 nm) was deposited on the GaN layer by e-beam evaporation and annealed at 850 °C for 30 s with a rapid thermal annealing system. Schottky contacts, with diameters in the range 50–400 μm, consisted of 50/150-nm Ni/Au stacks. They were deposited immediately after a dip in HCl to remove the thin oxide layer on the surface [33]. The best Schottky contacts were selected across the wafer on the basis of reverse-bias leakage current. All electrical measurements were done in the dark. The temperature measurements were carried out using a regulated Linkam heating/cooling silver stage mounted in a vacuum chamber and filled with 100 mbar 6N nitrogen gas. In this study, we investigated the 90–400 K range. Current-voltage-temperature (*I-V-T*) measurements were recorded with a Keithley 4200 Semiconductor Characterization System. Capacitance-voltage-temperature measurements at 1 MHz

were performed with a Boonton bridge (as part of a Phystech FT-1030 DLTS system) with a modulating signal of 100 mV. Some complementary C-V-T measurements at low temperatures were also realized with a HP 4192A LF impedance analyzer to estimate the effect of the parallel series resistance. This instrument was mainly used for the admittance spectroscopy in the frequency range $1 \times 10^3 - 1 \times 10^7$ Hz. The amplitude of the ac modulating signal was 100 mV. We performed frequency-dependent or temperature-dependent measurements of the conductance to extract the emission rate of deep levels versus temperature. The study was completed by the analysis of capacitance-temperature measurements at various frequencies, to check the consistency of the theory used. Complementary Van der Pauw/Hall measurements were performed with a Phystech RH-2010 system equipped with a closed-cycle He cryostat operating in the 10–300 K temperature range. Two light emitting diodes (LEDs) were mounted together with the sample for PPC experiments, and various LEDs color were used. Additional PPC experiments were conducted in a similar cryostat, using a high-pressure Xe lamp as light source and a Cornerstone monochromator coupled to an optical fiber for back illumination.

III. ELECTRICAL CHARACTERIZATION OF InAlN LAYERS

The electrical characterization presented here will concern mainly sample A described above. The results on sample B are very similar, except for a higher thermal activation energy of the deep level, probably related to the slightly lower In composition of sample B (Sec. IV).

A. Current-voltage-temperature characteristics and partial carrier freeze out

Typical dc (J-V_a-T) characteristics are shown in Fig. 1 for a few temperatures between 200 and 400 K, where J is the current density, V_a the applied voltage, and T the temperature. The room temperature reverse current density at -5 V of the selected diodes was 2.0×10^{-3} A/cm^2. Literature values are typically 10^{-2} A/cm^2 [34] or above [35], except in the publication by Chen *et al.* [9] where a reverse current density as low as 6.0×10^{-7} A/cm^2 at -5 V was reported. The forward characteristics of the current density J at low voltage ($\leqslant$1.2 V) follow an exponential dependence [36] on V_a for $T \geqslant 180$ K:

$$J = J_s e^{qV_a/E_0}(1 - e^{-qV_a/k_BT}), \quad (1)$$

where k_B is the Boltzmann constant, V_a is the applied voltage, E_0 is an energy parameter defined below, and J_s is a preexponential factor called saturation current density, extrapolated at zero bias. For biases larger than a few k_BT/q the second term in the bracket drops. The inset of Fig. 1 shows that E_0 does not change significantly with temperature, suggesting some tunneling mechanism. Padovani and Stratton [37] considered two temperature ranges to describe the regimes for the so-called field and thermionic-field emission. At low temperature, the field emission (direct tunneling) dominates and the saturation current does not depend strongly on T. The parameter E_{00} is an energy, which plays an important role in

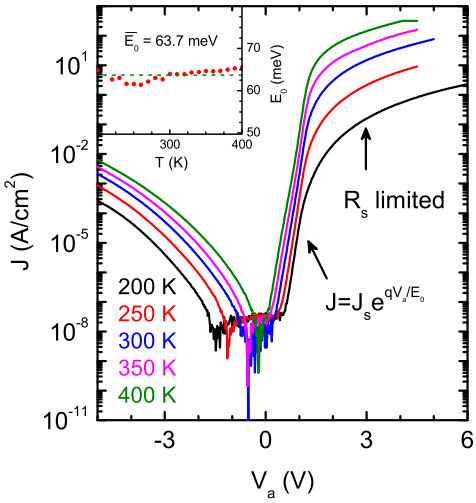

FIG. 1. (Color online) Experimental current density-voltage characteristics at various temperatures between 200 and 400 K. J increases with rising temperature. Actual ΔT steps were 10 K. Area of the Schottky contact $S = 3.14 \times 10^{-4}$ cm^2. The energy parameter E_0 [Eq. (1)] vs temperature is shown in the inset. Evaluation of the series resistance $R_s(T)$ was extracted from the linear dependence at high positive biases.

the tunneling theory. It is given by:

$$E_{00} = \frac{\hbar q}{2}\sqrt{\frac{N_D - N_A}{m^*\varepsilon_r\varepsilon_0}}, \quad (2)$$

where m^* is the electron effective mass in InAlN, ε_r is the relative static dielectric constant, ε_0 the permittivity in vacuum, q the electronic charge, and $\hbar$ the reduced Planck's constant. $N_D - N_A$ is the net residual doping near the surface, being different from the bulk value if the residual doping is nonuniform. At intermediate temperature range, on the other hand, J_s becomes strongly thermally activated, as observed experimentally (thermionic-field tunneling regime). In this region most of the electrons tunnel at an energy above the Fermi level in the semiconductor, but below the top of the large metal/semiconductor barrier Φ_B of 2.8 eV [33]. The energy parameter E_0, which appears in Eq. (1), is related to E_{00} by:

$$E_0(T) = E_{00}\coth(E_{00}/k_BT). \quad (3)$$

E_0 is almost constant against temperature (inset of Fig. 1). Thus, we can approximate E_{00} by the averaged value of E_0 (63.7 meV). The factor $\coth(E_{00}/k_BT)$, which appears in Eq. (3) indeed varies by only 5% between 180 K and 400 K. From Eq. (2), we deduce a net donor concentration of 3.3×10^{19} cm^{-3}, using $m^* = 0.28\ m_0$ and $\varepsilon_r = 10$. The value of m^* was estimated by a linear interpolation between the recommended values for AlN and InN [38]. The value of ε_r is compatible with our recent determination on InAlN/GaN HEMTs [33]. The obtained high doping level (3.3×10^{19} cm^{-3}) is an order of magnitude higher than the bulk value deduced from capacitance-voltage measurements taken in the low-frequency regime at depths in the range 15–43 nm and for V_a in the range [-5 V, 0 V]. The origin of this large difference between near surface and bulk donor concentrations might be due to the presence of a highly doped

thin surface barrier, originally proposed by Hasegawa and Oyama in GaN [39]. This model was successively applied to reproduce the I-V-T behavior of n-type GaN [39], n-AlGaN [40], and n-InGaN [41], illustrating that it is quite common to have a thin surface barrier in various nitrides. In InAlN, the presence of a highly doped thin surface barrier is compatible with dopant profiling by EC-V. Less probably, a high tunneling probability can result from a trap-assisted tunneling mechanism [33,42], if it still dominates in the forward direction and for large InAlN thicknesses.

The strongly thermally activated saturation current is now discussed in the framework of Padovani and Stratton [37] theory, with thermionic-field emission through the thin surface barrier. They derived an expression for $J_s(T)$ in terms of the Fermi level position in the semiconductor $E_F(T)$, the barrier height Φ_B, the energy E_{00}, and other physical constants. The dominant temperature dependence of J_s is given by:

$$J_s \propto \frac{T}{\cosh\left(E_{00}/k_BT\right)} e^{(E_F-E_C)/k_BT} \propto \frac{n_0(T)}{T^{1/2}\cosh\left(E_{00}/k_BT\right)}. \tag{4}$$

The last proportionality assumes a nondegenerate semiconductor, which seems justified by the high resistivity and the low electron concentration for low-In composition ($x < 0.4$) InAlN alloys at 300 K [13–16]. The dependence of n_0 versus reciprocal temperature is shown on Fig. 2(a). These data indicate a partial carrier freeze out, strongly suggesting the presence of a shallow (D_1) and a deep (D_2) level. The extracted activation energies are 77 and 263 meV for D_1 and D_2, respectively, by assuming a carrier concentration $n_0 \propto T^{3/2}e^{-E_a/k_BT}$ [see Eq. (12) and (13), Sec. IV for more details]. Note that these levels correspond to bulk states in the InAlN neutral region, as they fix the Fermi level position with respect to the minimum E_C of the conduction band in the InAlN layer [Eq. (4)].

The deep level D_2 is an important electrically active defect in our material as it becomes dominant above 250 K. An independent confirmation of our results can be obtained from the series resistance, although the data are more delicate to interpret quantitatively. The total series resistance R_s was extracted from the linear slopes of J-V characteristics (Fig. 1) at high forward bias (4.5–7 V). In principle, R_s contains several contributions. The first one comes from the n^+-GaN region and the Ohmic contact. It was evaluated by measuring both the sheet resistivity of a similar n^+-GaN layer, and the Ohmic contact resistivity and applying appropriate geometrical factors of the Schottky diode structure. This contribution lies between 15 and 20 Ω in the whole temperature range, almost negligible with respect to R_s, except at high temperatures. The influence of the reverse-polarized InAlN/n^+-GaN junction is less easy to assess, in absence of a detailed study of vertical transport through this junction at current levels used for our evaluation of R_s. Using the NEXTNANO3 simulator, we could estimate the junction barrier height Φ_{B2}, by using the same values of material parameters as Lugani *et al.* [33], a 3×10^{18} cm^{-3} doping for the n^+-GaN, and D_1 and D_2 concentrations in the InAlN layer as obtained by C-V measurements. The values found for Φ_{B2} are 100 meV at 100 K, 140 meV at 200 K, and 160 meV at 300 K. If the thermionic emission dominates,

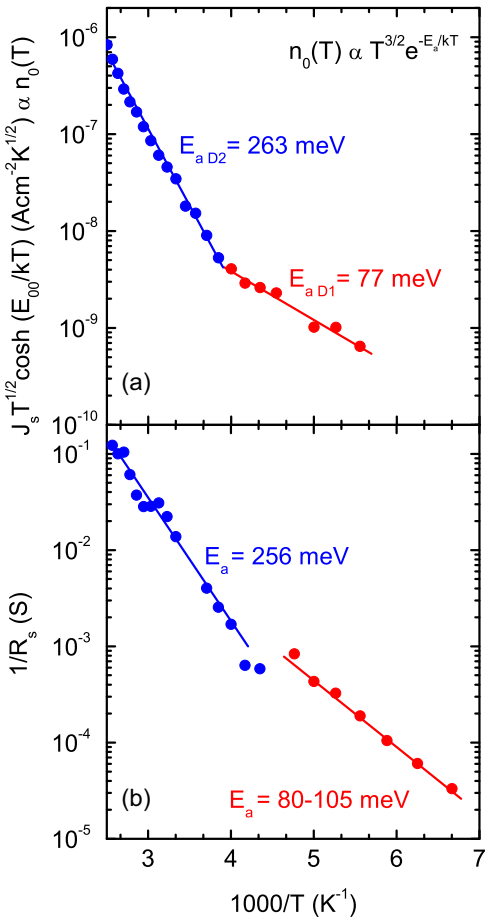

FIG. 2. (Color online) (a) Temperature dependence of the carrier concentration (arbitrary units) as deduced from the thermionic-field emission theory [see text and Eq. (4) for details]. (b) Reciprocal series resistance R_s versus inverse temperature. The activation energies refer to $n_0(T)$, assuming various temperature dependences of the mobility (see text).

the junction resistance would decrease exponentially with increasing temperature, with an activation energy given by Φ_{B2} [43]. For thermionic-field-emission or field-emission transport at reverse bias, the junction resistance is not thermally activated [37,43]. These results neglect any barrier height lowering by the reverse voltage, thus the simulated values constitute an upper limit for Φ_{B2}. This possibly activated resistance would play a role only if its contribution to the total resistance is relatively important and if the transport across the back junction is dominated by thermionic emission. In the absence of a detailed study of the vertical transport in such a junction, we are only able to discuss this point from the point of view of measured activation energies, as compared to those obtained from $n_0(T)$.

As for the carrier concentration, the series resistance decreases by more than three orders of magnitude between 150 and 400 K, as shown on Fig. 2(b) where $1/R_s$ is plotted versus inverse temperature. To give precise values of the ionization energies for D_1 and D_2, the temperature dependence of the electron mobility should be known. By assuming a $T^{-3/2}$ dependence for the mobility at high temperature, the

activation energy of D_2 is directly related to the slope of the upper branch, leading to a value of 256 meV. For the lower branch, the activation energy of the shallow level is found to be 105 meV if the low-temperature mobility is assumed constant, and 80 meV if the low-temperature mobility is proportional to $T^{3/2}$. Comparing the activation energies obtained by the two independent methods, there is a very good agreement for the deep level D_2 [Figs. 2(a) and 2(b)]. This supports a common origin for the upper branch. In other terms, the temperature behavior of R_s above 250 K is dominated by the resistance in InAlN, as could be expected from the large difference between its activation energy and the calculated value of Φ_{B2}. The lower branch is more delicate to discuss, since its activation energy is comparable to the expected values for Φ_{B2}. However, it is also comparable to the activation energy of $n_0(T)$, which is related to a shallow level (D_1) in bulk InAlN. We cannot exclude that the InAlN/n^+-GaN junction plays a role at low temperature. However, from the $n_0(T)$ dependence [Fig. 2(a)], we expect a quite resistive InAlN layer at low temperature. In this context, it is difficult to be quantitative about the respective contributions. In Sec. III C we will demonstrate some photoconductivity effect on R_s in this temperature range, which cannot be attributed to the back junction. In Sec. IV, we will discuss in more details Fig. 2(a), in particular the sharp break in slope, once the nature of the two levels will be better understood. The main goal of the following section is to confirm and characterize these two levels by admittance spectroscopy and to relate their signatures with the present data.

B. Admittance spectroscopy of InAlN layers

To further motivate the interest of performing admittance spectroscopy, it is worthwhile to examine the conductance and capacitance measured versus temperature at 1 MHz in the temperature range 100–400 K [Figs. 3(a) and 3(b)].

One observes two peaks, labeled D_1 and D_2, in the conductance. They are associated to inflexion points in the capacitance curves, much more pronounced for D_2 than for D_1. The positions of the peaks and inflexion points are almost independent of the applied voltage V_a in the range [−5 V, 0 V]. The peak amplitudes of both D_1 and D_2 increase by rising V_a. We assign D_1 and D_2 to thermally activated states in bulk InAlN, located in the upper half of the band gap, consistent with the interpretation of the temperature dependence of the saturation current. Anticipating on the results deduced from the admittance characterization of the two levels, the dependence of the thermal emission rate $e_n(T)$ versus temperature is also shown on Fig. 3(c) together with the position of the angular frequency at 1 MHz. This plot is useful to discuss the various frequency regimes of the capacitance. As discussed below, the conductance peaks and capacitance inflexion points appear when $\omega \approx e_n(T)$ [Figs. 3(a)–3(c)]. It is our objective to study the $e_n(T)$ dependence for D_1 and D_2, either by changing T or ω in such admittance measurements.

Since the pioneer work by Losee [44], admittance spectroscopy has been widely used to characterize slow responding levels in various Schottky-barrier junctions, by measuring the complex admittance as a function of temperature and/or frequency. The measurement conditions are usually close to the thermal equilibrium and the thermal emission rate is measured in a very narrow region of the space-charge region located at the crossing point of the Fermi level with the energy level of the center. An important caution in the admittance spectroscopy is

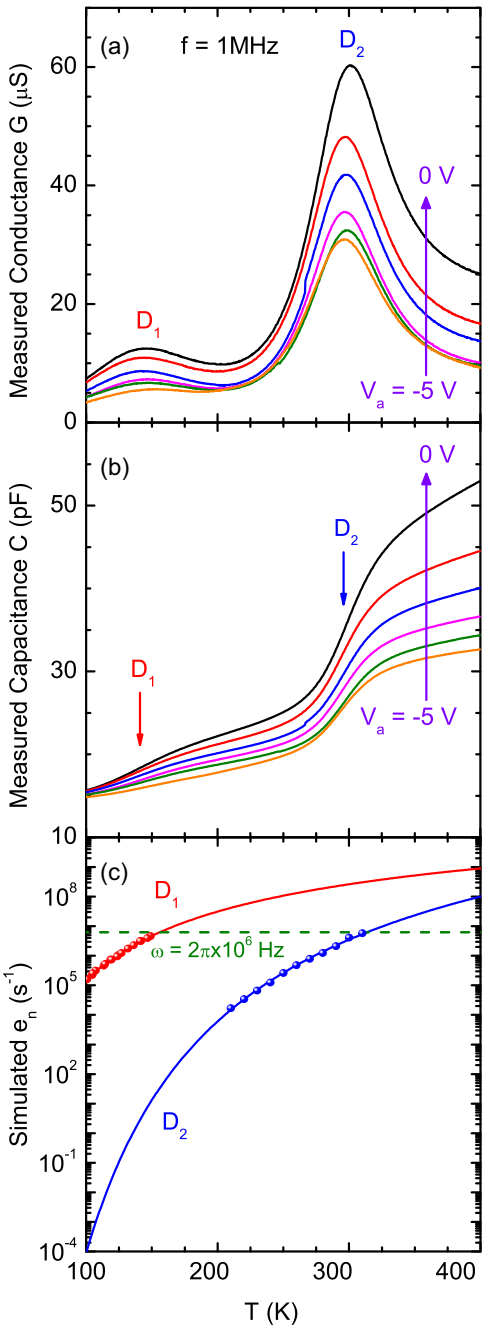

FIG. 3. (Color online) (a) Measured conductance G and (b) associated capacitance C at 1 MHz vs temperature at fixed applied voltages between −5 V and 0 V. Heating rate: 4 K/min, $S = 3.14 \times 10^{-4}$ cm^2. The two peaks in conductance and corresponding inflexion points in capacitance are attributed to a shallow donor D_1 and a deep level D_2. They appear when their emission rate $e_n(T)$ is comparable (see text) to ω. (c) Simulated emission rate e_n vs temperature from the parameters extracted from Fig. 6. This plot helps to define the various frequency regimes of the capacitance. The experimental points $e_n(T)$ are also displayed to visualize the regions of extrapolations.

to maintain the depletion width $W(V_a,T)$ below the thickness of the InAlN layer. Under these conditions, no spurious effects are expected from the 2DEG at the InAlN/n^+-GaN interface, as confirmed by C-V-T data analysis. Also, the possible surface states at this interface should not play a role in our measurements. It is worth noting that both D_1 and D_2 appear at all biases between −5 V and 0 V [Fig. 3(a)], not simply below a certain bias as expected if states at the interface were playing a significant role in our measurements. We thus consider a simple equivalent circuit model consisting of a junction (capacitance C and conductance G in parallel) in series with the resistance $R_s(V_a,T)$. The series resistance has the same nature as for the diode characterization, except that the length of the neutral InAlN region is now shorter and more temperature dependent because of $W(V_a,T)$. The theory by Dueñas *et al.* [28] for a single deep center of emission rate $e_n(T)$ predicts that for $\omega \approx e_n(T)$, the conductance $G(\omega,T)$ is given by:

$$G(\omega,T) = \frac{C_{\rm LF} - C_{\rm HF}}{2} e_n \ln\left(1 + \frac{\omega^2}{e_n^2}\right). \quad (5)$$

Equation (5) assumes, which is usually the case, that the emission rate is much smaller than the capture rate in the neutral region at any experimental temperature. $C_{\rm LF}$ and $C_{\rm HF}$ are the capacitance in the low-frequency [$\omega \ll e_n(T)$] and in the high-frequency [$\omega \gg e_n(T)$] regimes respectively. Equation (5) is also valid in presence of a shallow donor, as derived by Barbolla *et al.* [45] in the extension of the original theory [28]. Their derivation was developed for an acceptorlike deep center [charge states (−,0)]. Qualitatively, the amplitude of the peak D_2 as a function of the applied voltage [Fig. 3(a)] is in agreement with the dependence of $C_{\rm LF} - C_{\rm HF}$ upon V_a shown on Fig. 3(b). Peak D_1 has a smaller amplitude, in relation with the smaller value of $C_{\rm LF} - C_{\rm HF}$ for this level. For both traps, their thermal emission rate can be evaluated at the temperature $T_{\rm max}$ corresponding to the conductance maximum, satisfying [28,45]:

$$e_n(T_{\rm max}) = \omega/1.98, \quad (6)$$

for a fixed angular frequency ω. Repeating the conductance measurements $G(T)$ at other ω values allows to study the dependence $e_n(T)$. This is the principle of thermal admittance spectroscopy, and some experimental curves are shown on Fig. 4 for an applied voltage fixed at −3 V. Since $e_n(T_{\rm max})$ is proportional to ω it is preferable, for scaling reasons, to plot G/ω versus T (Fig. 4). Conductance spectroscopy of the weak D_1 level was done in this way. We also applied this method to the D_2 level, and checked the consistency of our results with frequency-dependent admittance spectroscopy.

In the frequency admittance method, on the other hand, G/ω is measured versus ω at a fixed temperature T. This is shown on Fig. 5 for level D_2, only steps of 20 K being displayed for sake of clarity. Again, these data were recorded at $V_a = -3$ V. Equation (5) predicts a peak of (G/ω) at $\omega_{\rm max}$ such that [28,45]:

$$e_n(T) = \omega_{\rm max}/1.98. \quad (7)$$

The advantage of this method over thermal admittance spectroscopy is that the measurements are taken at a fixed

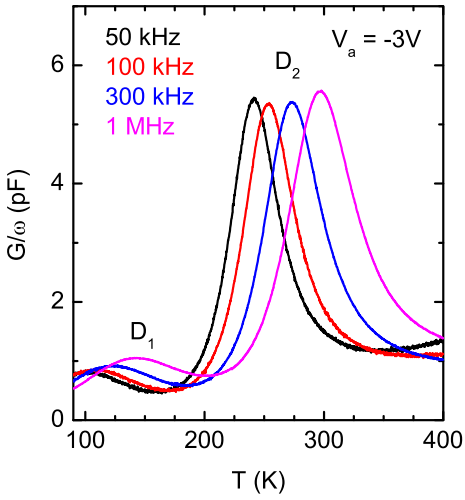

FIG. 4. (Color online) Measured G/ω vs. temperature for a few frequencies, at a fixed applied voltage of −3 V. The G/ω peaks shift towards higher temperatures with increasing frequency. The Arrhenius plot for D_1 was built from such thermal admittance experiments. Heating rate: 4 K/min, $S = 3.14 \times 10^{-4}$ cm^2.

temperature T. It is thus easier to correct (see Appendix) for the series resistance $R_s(T)$, the measured conductance obtained in a parallel circuit configuration mode [46]. For six sets of $e_n(T)$ data taken at different applied voltages in the range [−5 V, 0 V], the incidence of R_s on the thermal activation energy E_{a,D_2} [obtained from Eq. (8), see later] of the D_2 level was found to be very small, i.e., a reduction of less than 3% compared to the uncorrected data.

These measurements of $e_n(T)$ allowed to build Arrhenius plots for the two levels. These plots are based on the dependence of $e_n(T)$ deduced from the detailed balance

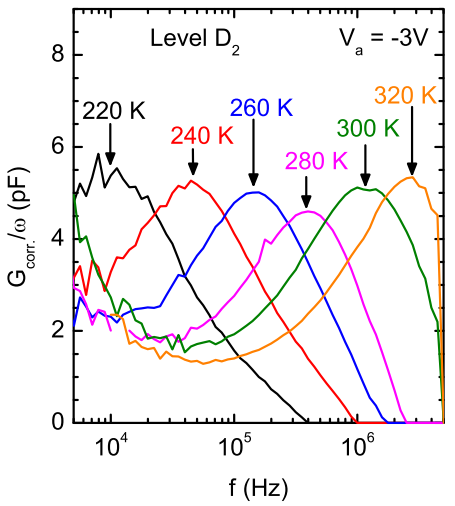

FIG. 5. (Color online) $G_{\rm corr}/\omega$ versus frequency at fixed temperatures and fixed applied voltage V_a. $G_{\rm corr}$ is the corrected conductance for the effect of the series resistance $R_s(T)$ in a parallel mode of measurement. The Arrhenius plot for D_2 was built from such frequency-dependent admittance experiments. $S = 3.14 \times 10^{-4}$ cm^2.

equation [47]:

$$e_n(T) = \sigma_{nD} v_{th}(T) e^{(\alpha_D/k_B)} \frac{1}{g_D} N_C(T) e^{-E_{aD}/k_B T}, \quad (8)$$

where σ_{nD} is the thermal capture cross section of an electron in the conduction band by the level D (D_1 or D_2), v_{th} is the mean thermal velocity of free electrons ($\propto T^{1/2}$), N_C is the effective density of states at the minimum of the conduction band ($\propto T^{3/2}$), g_D the degeneracy factor for the donor level D, and E_{aD} its thermal activation energy. In the absence of more information, the factor e^{α_D/k_B}, related to the negative linear temperature dependence of the energy level ($E_D = E_{D_0} - \alpha_D T$), was taken to be 1 (i.e., $\alpha_D \approx 0$). If the capture cross section σ_{nD} is not thermally activated, the thermal activation energy corresponds to the energy depth of the level ($E_C - E_{D_0}$) and the preexponential factor contains a T^2 dependence. Our quoted values of σ_{nD} based on Eq. (8) assume a degeneracy factor g_D of 2 and an effective mass $m^* = 0.28\ m_0$. The Arrhenius plots of e_n/T^2 in log scale versus inverse temperature are shown on Fig. 6. The slope and the intercept on the vertical axis (at $T \to \infty$) of each straight line give the following signatures: thermal activation energy $E_{aD_1} = 68$ meV, $\sigma_{nD_1} = 9.7 \times 10^{-17}$ cm^2 for D_1, and $E_{aD_2} = 290$ meV, $\sigma_{nD_2} = 6.2 \times 10^{-15}$ cm^2 for D_2. Similar results were obtained by the thermal admittance method on D_2, which confirms the low impact of $R_s(T)$.

Note that the emission rate of D_2 at 300 K is about 7×10^6 s^{-1}, much faster then values reported by Arslan *et al.* for surface states in InAlN/AlN/GaN heterostructures [48]. From their frequency-dependent admittance measurement at room temperature, they found emission rates of $1.4 - 3.3 \times 10^5$ s^{-1} for an unpassivated structure, and slightly higher values of $5 - 5.5 \times 10^5$ s^{-1} for a sample with an SiN_x layer between the metal contact and the InAlN layer. This large difference between emission rates in both studies indicates that D_2 is not related to their surface states. The same conclusion holds for D_1, which is even faster than D_2 at 300 K.

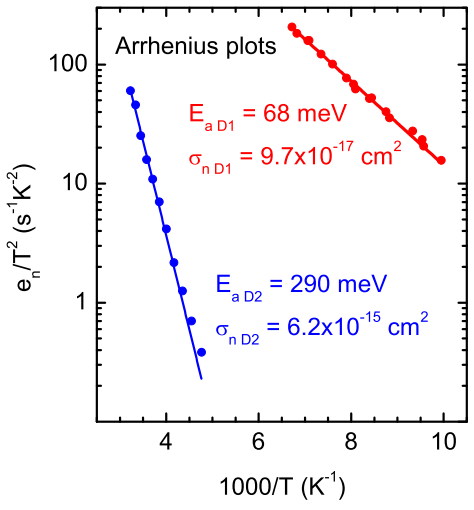

FIG. 6. (Color online) Arrhenius plots for the two levels with their signatures, deduced from the admittance spectroscopy data taken at $V_a = -3$ V. The values of capture cross sections assume $m^* = 0.28\ m_0$ and $g = 2$. D_1 points are obtained from thermal admittance spectroscopy, D_2 points from frequency-dependent admittance spectroscopy.

Furthermore, for the deep level D_2, Arrhenius plots were also obtained from data taken at other applied voltages in the range [−5 V, 0 V] (data not shown here). There is some very small variation of E_{aD_2} with V_a, by a maximum of 15 meV between −5 V and −1 V. It could result from slight nonuniformities of the indium composition across the explored depth (see Sec. IV). It probably does not result from the Poole-Frenkel effect [49]—acting only in the case of a donorlike D_2 center, but not in the case of an acceptorlike D_2 center—as the electric field at the crossing point between E_D and the Fermi level E_F is not influenced significantly by V_a.

Concerning the activation energy of the shallow D_1 level, the data are based on the conductance measurements versus temperature in the range 90–180 K, at various fixed frequencies between 71 kHz and 1.44 MHz (Fig. 4). The amplitude of the D_1 peak depends on V_a in the same way as for the D_2 peak, indicating that corrections to the conductance due to series resistance associated effects are still small. However, we could not correct the measured conductance for the series resistance effect because $R_s(T)$ is not known in the 90–180 K range from J-V measurements and because the temperature and voltage-dependent length of the neutral InAlN region should be taken into account. In order to qualitatively estimate the effect of $R_s(T)$, its value was extrapolated in the 90–180 K range from data in the 190–250 K range [Fig. 2(a)]. Conductance corrections follow the equations given in the Appendix. The results show that the true conductance peak is shifted at a higher temperature, which allowed us to evaluate the effect on the Arrhenius plot. The net effect of R_s related corrections is a slight increase of the thermal activation energy and a more significant decrease of the thermal capture cross section. Anyhow, our determination of E_{aD_1} agrees pretty well (within 12%) with the activation energy deduced from the temperature dependence of the saturation current (Sec. III A).

For both levels, the thermal activation energies (Fig. 6) are close to those found by the analysis of the saturation current [Fig. 2(a)]. This strongly suggests that the same levels were studied by admittance spectroscopy in the junction region and by analysis of the temperature dependence of $n_0(T)$ in the neutral region. Furthermore, the activation energy for D_2 level is about 27 meV larger than in the I-V-T measurements. If this is not due to an In nonunifomity in the sample, it could result from an activated capture cross section [47], with an activation energy $E_\sigma \approx 27$ meV. The data for D_1 are less accurate due to the various experimental errors (small J_s, few data points for the I-V-T data, large R_s, uncertainty on the correction of the admittance data by an appropriate series resistance).

The parameters obtained from the Arrhenius plots allow a simulation/extrapolation of their emission rates versus temperature thanks to Eq. (8). This was shown in the range 100–400 K on Fig. 3(c), with the position of the angular frequency corresponding to $f = 1$ MHz. This plot is very useful to visualize the T regions corresponding to the high- and low-frequency regimes of the capacitance [Fig. 3(b)], usually measured at 1 MHz. The frequency dispersion of the capacitance [$\omega \approx e_n(T)$] for a single deep level was derived

by Dueñas *et al.* [28], together with Eq. (5):

$$C(\omega,T) = C_{\mathrm{HF}} + (C_{\mathrm{LF}} - C_{\mathrm{HF}})\frac{e_n}{\omega}\arctan\frac{\omega}{e_n}, \qquad (9)$$

where C_{HF} and C_{LF} are the high-frequency ($\omega \gg e_n$) and low-frequency ($\omega \ll e_n$) capacitance, respectively. Barbolla *et al.* [45] showed that the frequency dependence $C(\omega,T)$ in the intermediate-frequency regime (near $\omega \approx e_n$) is not modified by the presence of shallow donors, if appropriate expressions for C_{LF} and C_{HF} are used. To corroborate this result, Dhariwal and Deoraj [50] derived a slightly more complicated functional dependence than found in Eq. (9), but their corrective term becomes negligible for $e_n \approx \omega$. The exact criteria for getting a pure LF or HF regime is embedded in Eq. (9). The frequency factor $(e_n/\omega)\arctan(\omega/e_n)$ varies between 0 and 1, corresponding to pure HF and LF regimes at low T and high T respectively. For instance, the LF regime for the deep level D_2 is obtained above 350 K for $f = 1$ MHz.

The temperature dependence of the capacitance, at a constant frequency [Eq. (9)], exhibits an inflexion point at a temperature T_i, sometimes used to characterize the deep level according to [28,45]:

$$e_n(T_i) = \omega/1.825. \qquad (10)$$

The functional dependence given by Eq. (9) explains very well our measurements in the intermediate regime of the deep center D_2. Figure 7 shows the measured C-T characteristics at $V_a = -3$ V and at three frequencies 10 kHz, 100 kHz, and 1MHz. At high and low temperatures, we do not expect a frequency dependence of the capacitance in the ideal case $R_s = 0$, since we are in the low-frequency and high-frequency regimes respectively [Fig. 3(c)]. The observed small reduction of the measured capacitance with increasing frequency is due to the finite value of R_s. Figure 7 shows that the smoothed capacitance step shifts towards higher temperatures for higher frequencies, as expected by Eq. (10). These C-T curves were simulated by inserting in Eq. (9) the dependence $e_n(T)$ [Fig. 3(c)] deduced from the Arrhenius plot. We also superimposed the experimental linear temperature dependence, likely due to C_{HF}. The only fitting parameter in Eq. (9) was the amplitude of the step $C_{\mathrm{LF}} - C_{\mathrm{HF}}$, which turns out to be 11.2 ± 0.8 pF at $V_a = -3$ V and for the three frequencies. The same value is deduced from the maximum of $G(\omega,T)$ at -3 V [Fig. 3(a)], after applying a small correction (5%) on the amplitude of the peak due to R_s at 300 K. As shown on Fig. 7, the agreement between theory and experiment for $C(\omega,T)$ is excellent.

C. Persistent photoconductivity effects

It will be shown elsewhere that the D_2 center has a sluggish kinetics at low temperature, evidenced by hysteresis in the C-V_a loops obtained by sweeping the applied voltage in the up and down directions.

We now demonstrate PPC effects in two types of samples incorporating InAlN nearly lattice-matched to GaN. In the first example (sample B, very similar to sample A) we studied the I-V-T of a Schottky diode in the temperature range 100–300 K. After measuring the I-V-T characteristics in the dark by rising the temperature in steps of 10 K and waiting about 5 min for stabilization, the sample was cooled again at 100 K, then back illuminated by a subband gap (2 eV) monochromatic light. The exposure to light shifted upward the measured I-V curves and once saturation was reached, the illumination was switched off. The sample was allowed to relax for any fast recovery, and stable characteristics were reached after about 5 min. The I-V-T characteristics were then measured in the dark in this so-called PPC state. The extraction of the series resistances was done in dark and in the PPC state. The results are shown on Fig. 8. Indeed, a persistent effect is observed on the total series resistance at low temperatures. Approximatively, the PPC effect persists till

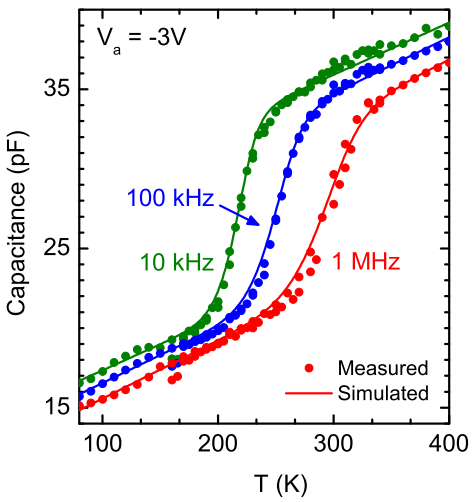

FIG. 7. (Color online) Simulated frequency dispersion of the capacitance in the intermediate-frequency regime for the D_2 level. The experimental linear temperature dependence, likely due to C_{HF}, was included in Eq. (9) and $e_n(T)$ was calculated as in Fig. 3(c). $S = 3.14 \times 10^{-4}$ cm^2.

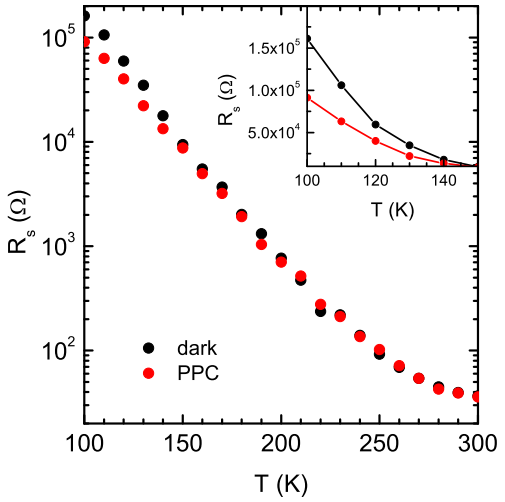

FIG. 8. (Color online) Series resistance R_s of an InAlN/n^+−GaN Schottky diode (sample B) in the dark. The data are taken before (black points) and after (red point) illumination at 100 K by a subband gap (2 eV) monochromatic light. A PPC effect is clearly seen at low temperature. $S = 1.26 \times 10^{-3}$ cm^2.

a temperature $T_c \approx 150$ K. Note however that the temperature is not well controlled in this experiment, since the poor heat dissipation in our particular setup for back illumination and the relatively large power dissipation at voltages above 6.5 V for determining R_s. This qualitative observation is a strong indication for the presence of a DX-like center in InAlN nearly matched to GaN, presumably D_2 due to its hysteresis behavior observed by C-V-T.

PPC effects were also demonstrated using the HEMT heterostructure, where exposure to light affects the sheet carrier density of the 2DEG. This experiment does not suffer from temperature control, as above, as the sample was mounted on a gold-plated copper block, the current was below 3.4 μA and the illumination by the LEDs could be performed from the front, with no need for a large hole in the block for back illumination. Figure 9 shows experiments at 15 K where the evolution of the sheet carrier concentration n_s is recorded versus time, with the following sequence: first in the dark (Off), then under illumination (On) and finally in the dark (Off). Note that the values of n_s in the dark slightly differ, depending on the history of the sample (aging, previous illumination in particular). For the illumination, we used LEDs with peak photon energies of 1.4, 2.0, and 2.6 eV. There is almost no change of n_s under infrared illumination (1.4 eV). Both red (2 eV) and blue (2.6 eV) light induce instead a clear rise of n_s, which persists after switching off the light. The mechanism at low temperature is the following: if the photoexcited deep center has a slow thermal capture rate at that temperature, the photoexcited electrons can tunnel through the thin AlN barrier into the 2DEG gas, increasing its concentration. Although not corrected for the photon fluxes, the rise time during illumination is much faster for the blue light than for the red light, as expected from the dependence of the optical cross section with photon energy of the deep center [51]. If we look more closely the data for the blue light, there is a tiny decay of n_s in the PPC state, indicating that a small fraction of photoexcited electrons decay at a relatively fast rate compared to the major part. Otherwise, there is a clear persistence of n_s at 15 K, with no sign of decay during 1 hr or more. The value of $\Delta n_s = n_{s,\mathrm{PPC}} - n_{s,\mathrm{dark}}$ is 9.5×10^{11} cm^{-2} for the red light and 1.05×10^{12} cm^{-2} for the blue illumination. This very small difference is a strong indication that the origin of the observed PPC effect is not related to photoexcited carriers located in a continuum of surface states. Thus, the defects responsible for the PPC effect should be located in the barrier, since we did not observe PPC effect in n^+-GaN, at least with the red light. This conclusion is consistent with the change in R_s discussed before (Fig. 8). With a barrier of 5nm (AlN + InAlN) the concentration of the metastable center responsible for the PPC effect in the thin heterostructure sample is estimated to be 2×10^{18} cm^{-3}. We then performed temperature Hall measurements in the dark, and in the PPC state, by sweeping the temperature at a 85 K/hr rate, steps of 3–4 K. The result for n_s and mobility μ in the 10–300 K range are shown in Fig. 10, both in the dark and in the PPC conditions after illumination with red LEDs. Below 100 K, Δn_s is stable, then gradually decreases. Even at 300 K, Δn_s does not vanish, indicating some slow kinetics. Concerning the mobility, they are typical for a 2DEG gas. The increase in mobility in the PPC state is not very pronounced, probably due to the onset of occupation of the second subband in this n_s range.

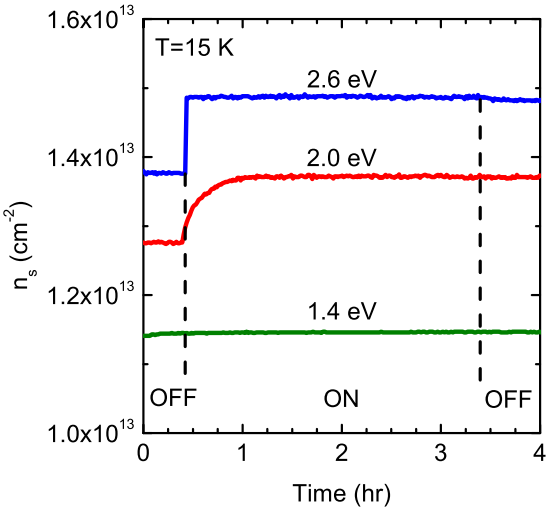

FIG. 9. (Color online) 2DEG sheet carrier concentration n_s at 15 K versus time measured on a thin barrier InAlN/AlN/GaN heterostructure. The time sequence for illumination was: dark (OFF), illumination (ON), dark again (OFF, PPC state). Three experiments were performed at various photon energies. A PPC effect is clearly seen after illumination at 2 or 2.6 eV. The variations of n_s in the dark depend on the history of the sample.

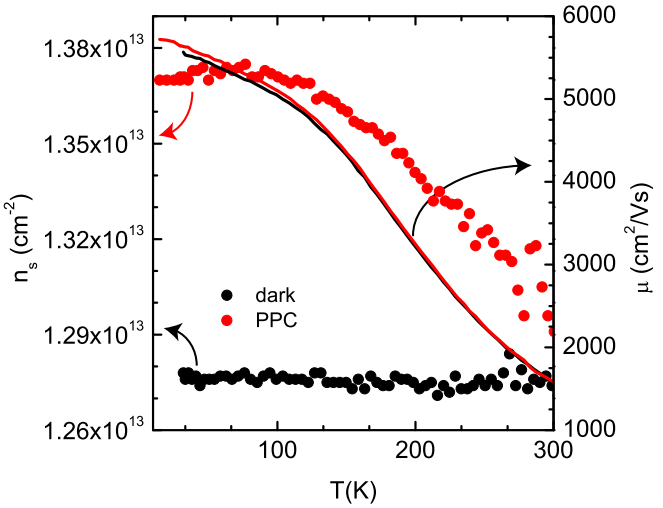

FIG. 10. (Color online) 2DEG sheet carrier concentration n_s and Hall mobility μ in the dark versus temperature following sufficient photoexcitation at 2 eV to reach saturation of n_s at 15 K. The sample used was the same as in Fig. 9.

IV. DISCUSSION OF THE SHALLOW AND DEEP LEVELS

We discuss in this section the main results concerning the two observed levels. The shallow level has a thermal activation energy of about 68–77 meV and a capture cross-section 9.7×10^{-17} cm^2. Its emission rate at 150 K is 4.7×10^6 s^{-1} [Fig. 3(c)], and thus, cannot correspond to the shallowest level (0.164 eV) reported by DLTS, with emission rate of 110 s^{-1} at 150 K [25]. To our knowledge, the D_1 level was not yet reported

in InAlN. We attribute D_1 to a hydrogenic state of an impurity, most likely oxygen occupying a nitrogen site, as suggested by the concentrations given by E-CV (low-frequency CV) and by SIMS. This point will be further developed elsewhere, by extracting the concentrations of D_1 and D_2 from the C-V-T measurements. The activation energy of 68–77 meV is higher than the effective Rydberg (38 meV) calculated under the assumptions $m^* = 0.28\ m_0$ and $\epsilon_r = 10$. Tansley and Egan [52] predicted higher effective Rydberg of donors in polar semiconductors such as nitrides. A simple linear interpolation between their values for InN (23 meV) and AlN (200 meV) gives 170 meV for $In_{0.16}Al_{0.84}N$. Our experimental value lies between the simple and refined theory.

The D_2 level center has an activation energy of 290 meV and a cross section of 6.2×10^{-15} cm^2 (3.1×10^{-15} cm^2 for $g_{D_2} = 1$, usually assumed in DLTS studies). As mentioned before, the larger value of the activation energy obtained by admittance spectroscopy than by Fig. 2 may be due to an activated electron cross section. We measured another 200-nm-thick InAlN sample with a slightly lower In composition, 15.4% (sample B) instead of 16.1% (sample A) and found a thermal activation energy of 322 meV and a capture cross section of 8.2×10^{-15} cm^2. The small difference in capture cross section is not significant, as a small error in the slope of the Arrhenius plot can induce a noticeable change in σ deduced from the vertical intercept. The variation in activation energy indicates a sensitive effect of the indium composition and/or of its related tensile strain. Although the In compositions are very close, we note that the difference in energy of 32 meV corresponds to 2/3 of the InAlN band-gap variation predicted by Gorczya *et al.* [53] for a uniformly In distribution (i.e., nonclustered, bowing parameter $b = 2.1$ eV). This absence of pinning to the conduction band, also observed in AlGaN, is consistent with a strong localization of the deep state wave function in real space [22]. More pragmatically, the dependence of the energy depth upon indium composition should be kept in mind when comparing our data with other studies, done at slightly different indium compositions. Chikhaoui *et al.* [27], using current-DLTS on HEMTs, reported a level with signature of 365 meV and $\sigma = 1.4 \times 10^{-19}$ cm^2. This level cannot correspond to the D_2 center, considering the huge discrepancy in capture cross sections. In a high-quality 130-nm-thick sample having 17.65% In, Chen *et al.* [26] reported three levels (E_1–E_3) by spectrum fitting their broad DLTS peak. The e_n/T^2 value at 250 K of our D_2 level lies between the extrapolated values at 250 K for their E_1 and E_2 levels. Chen *et al.* quote the following signatures: activation energy of $E_1 = 351$ meV and a cross section $\sigma = 4.0 \times 10^{-17}$ cm^2 for E_1, $E_2 = 404$ meV, $\sigma = 1.3 \times 10^{-15}$ cm^2 for the level E_2 (m^* and degeneracy factor not specified). The energies are slightly larger than E_{aD_2}, despite the larger indium composition. However, as the two techniques are different and cover different emission/temperature ranges, it is plausible that D_2 corresponds to E_2 (better agreement in terms of the cross section), or an unresolved combination of E_1 and E_2. Finally, the signature of the D_2 level is very similar to the level found by thermal admittance spectroscopy by Johnstone *et al.* [25], with thermal activation energy of 350 meV and $\sigma = 9 \times 10^{-15}$ cm^2 ($g = 1$, m^* not specified). Compared to our study, there are some technical differences in the analysis of the thermal admittance data and in the indium composition, quoted to be 18% for their sample. Quite interestingly, they observed an overlap, with transition in slope, in the Arrhenius plot obtained by thermal admittance spectroscopy and the one obtained by DLTS for a trap with an activation energy of 164 meV and a cross section $\sigma = 9 \times 10^{-19}$ cm^2. The possible relation between the two levels was further confirmed by capture measurements [25]. Unfortunately, no physical interpretation was proposed for this observation. As for D_2, their concentration of the DLTS trap was 1.6×10^{18} cm^{-3} for a residual doping as high as 4×10^{19} cm^{-3} (measured though below 10 nm, thus in the thin surface barrier). Another interesting result from their work comes from the lack of field dependence in the double-pulse DLTS experiments at 150 K for the dominant slow and fast components of their DLTS peak at 150 K. They concluded that the two traps are acceptorlike.

The concentration of D_2 should be high, since it dramatically affects the carrier concentration above 250 K. It was confirmed by the PPC measurements on the thin barrier heterostructure (averaged value for the InAlN/AlN barrier of 2×10^{18} cm^{-3}). It is metastable, as evidenced by PPC effects, similar to the behavior of DX centers in other semiconductors. We also know that our samples contain a high concentration of oxygen (as evidenced by SIMS) and that DX centers associated to oxygen are indeed predicted in AlN [19–24] and AlGaN [19–23] for $x \geqslant 0.6$. Experimentally, O-related DX centers were demonstrated in AlGaN, at Al compositions as low as 0.39, with an extrapolated onset at 0.3 [21,22]. They can occur in our samples, because of the large band gap of 4.5 eV for nearly lattice-matched InAlN. These deep states are associated to the so-called DX centers [17,18] induced by a bond-breaking distortion at a substitutional nitrogen donor site. The density of DX centers can be high, up to one-half the density of the donor atoms [18], naturally explaining the high density of the D_2 center estimated from the PPC experiment on the thin barrier sample. We also observed hysteresis in the C-V_a curves at low temperatures as in other semiconductors containing DX centers. The ground state of DX centers is negatively charged (DX^-) [19–24] in agreement with the acceptorlike behavior reported by Johnstone *et al.* [25]. More experimental facts, such as the determination of D_1 and D_2 concentrations, are needed to attribute the deep level D_2 to an O-related DX center, but the above discussion points out that it is a likely candidate.

The presence of DX centers allows us to explain the temperature dependence of the carrier concentration $n_0(T)$ [Fig. 2(a)]. In our data two branches, hereafter referred to as upper (above 250 K) and lower (below 250 K) branch, appear with an abrupt change in slope at about $T_f = 250$ K, i.e., without smooth transition between the two slopes. Such a peculiar phenomenon has also been observed in AlGaAs:Si [54,55] and explained by Theis *et al.* [54]. Quite generally, the concentration of free carriers in the neutral region is given by:

$$n_0 = n_{D_1^+} - n_{D_2^-} - N_A, \tag{11}$$

where $n_{D_1^+}$ is the concentration of ionized shallow donors and $n_{D_2^-}$ is the concentration of negatively charged DX states. A multilevel statistics is necessary to describe these quantities, since they have the same chemical origin (likely oxygen in our case) and are therefore not independent. In Theis *et al.*'s treatment, the degeneracy factors were taken equal to 1.

Inclusion of degeneracy factors can be found in more recent publications for AlGaAs [56–58], GaAsP [56], and CdF_2 [59], but the basic physics is not fundamentally changed. The relevant physical quantities in their expressions of occupancies are the respective Gibbs energies $\Delta\mathcal{G}_D = \Delta H_D - T\Delta S_D$ for transfer from the appropriate level to the lowest-lying band edge, and the total dopant concentration N_D ($\equiv N_{D_1} + N_{D_2}$). Since the separation between the D_1 and D_2 level exceeds several k_BT over the whole temperature range considered, the deep level contribution dominates at high T and according to Theis *et al.* [54] and McCluskey *et al.* [22], n_0 in the upper branch is solution of the implicit equation:

$$n_0 = \sqrt{\frac{N_D - N_A - n_0}{N_D + N_A + n_0}} N_C\, e^{-\Delta\mathcal{G}_{D_2}/k_BT}. \qquad (12)$$

In the low-temperature limit of this branch, i.e., $n_0 \ll N_D - N_A$, Eq. (12) becomes explicit because the square-root term reduces to a constant, and $n_0(T)$ has a $T^{3/2}e^{\Delta S_{D_2}/k_B}e^{-\Delta H_{D_2}/k_BT}$ temperature dependence, where ΔH_{D_2} is the difference in enthalpy between the conduction band minimum and the D_2 level. If the entropy contribution $e^{\Delta S_{D_2}/k_B}$ does not change significantly with temperature, the prefactor of the exponential term has a $T^{3/2}$ dependence (from N_C), which is used for the the fitting of the data of Fig. 2(b). The abrupt change in slope between the two branches has been explained by Theis *et al.* assuming that the DX center abruptly ceases to equilibrate with the band edge and the hydrogenic level below a temperature T_f, which corresponds to the break in slope. In other terms, only the shallow levels are in equilibrium with the conduction states, while $n_{D_2^-}$ is frozen to its value at $T = T_f$. In this situation, n_0 is solution of the implicit equation [54]

$$n_0 = \frac{N_D^{\text{eff}} - N_A^{\text{eff}} - n_0}{N_A^{\text{eff}} + n_0} N_C e^{-\Delta\mathcal{G}_{D_1}/k_BT}. \qquad (13)$$

Equation (13) is a standard formula for a semiconductor with a single type of donor and a background of acceptors, except for the important corrections $N_D^{\text{eff}} = N_D - n_{D_2^-}(T = T_f)$ and $N_A^{\text{eff}} = N_A + n_{D_2^-}(T = T_f)$. The lower branch saturates hypothetically at high temperature at a value $N_D^{\text{eff}} - N_A^{\text{eff}} = N_D - N_A - 2n_{D_2^-}(T = T_f)$, which can be much lower than $N_D - N_A$. We note that n_0 is $\ll N_A^{\text{eff}}$ for the lower branch. Furthermore, the product $N_Ce^{-\Delta H_{D_1}/k_BT}$ is $\ll N_A^{\text{eff}}$ because the exponential term is only 4.26×10^{-2} at the maximum temperature $T = 250$ K, whereas N_A alone [i.e., without the additive term $n_{D_2^-}(T = T_f)$] is already of the order of $N_C(250\text{ K})$. In this case, Eq. (13) becomes explicit and $n_0(T)$ has an activation energy equal to the enthalpy energy of the hydrogenic level. The prefactor is proportional to $T^{3/2}$, as used in our analysis of the lower branch. This is not a surprise as the material becomes highly compensated in this lower branch. Note that the values of n_0 given by Eqs. (12) and (13) should match at 250 K. As a consequence, considering the large difference in activation energies for D_1 and D_2, we reach the conclusion that $n_{D_2^-}(T = T_f)$ is only slightly less than $(N_D - N_A)/2$, in agreement with the mechanism of formation of DX centers [18].

V. SUMMARY AND CONCLUSION

The major results of this paper concern the characterization by admittance spectroscopy of a shallow donor D_1 and a deep level D_2 in nearly lattice-matched InAlN to GaN. The DX-like nature of a defect, most likely the dominant D_2 electrically active center, is shown by the evidence of a PPC effect. It is suggested that D_1 and D_2 might correspond to oxygen in two distinct lattice configurations, the substitutional one (N site) being the hydrogenic state D_1 whereas a lattice-distorted configuration gives rise to a deep DX center. The presence of D_2 as DX center allows a qualitative interpretation of the temperature dependence of the carrier concentration, as extracted from the I-V-T diode characteristics in the thermionic-field emission regime. Clear partial carrier freeze out is observed, with a dominant contribution of the deep center above $T_f \approx 250$ K. According to Theis's theory [54], the occupation of the DX centers is frozen below T_f, i.e., no more in thermal equilibrium with conduction band states and shallow levels. Finally, based on existing theories, some aspects of the temperature and of the frequency dependences of the capacitance were discussed in presence of a deep center D_2 whose concentration is less than, but comparable in magnitude to, the shallow donor concentration D_1.

As future work, more persistent photoconductivity experiments, C-V_a hysteresis analysis, and photocapacitance experiments should provide useful insights on the metastability of the D_2 center. Its electronic structure should be investigated by complementary techniques such as Laplace transform DLTS. In the context of proposed deep DX centers, a multilevel structure is expected from the inequivalent orientations of the broken bond in the wurtzite structure [23,24] and also because the alloy material allows various local atomic configurations in the occupation by In and Al atoms surrounding the dopant. This local alloy disorder effect is known in Si-doped $Al_xGa_{1-x}As$ [60] even with a diluted Al composition [61] ($x = 0.04$ and 0.08, experiments under pressure). For such studies, it would be useful to characterize thinner samples with improved crystalline quality [30]. The impact of the indium composition, and its related strain state on the appearance and energy levels of the D_2 center should also be further investigated.

ACKNOWLEDGMENTS

This work was supported by the Swiss National Science Foundation through Grants No. 200021-132096 and No. 200020-147142.

APPENDIX

In the ideal case the admittance of a Schottky junction is modeled by a parallel combination of a capacitance and a conductance. However, a more realistic equivalent circuit should include a series resistance R_s. This introduces a difference between the capacitance and conductance measured in a parallel configuration mode (denoted here as C and G, respectively) and the true capacitance and conductance C_{corr} and G_{corr}. The relation between these quantities can be obtained by solving the standard formulas $C(C_{\text{corr}}, G_{\text{corr}}, R_s)$

and $G(C_{\rm corr}, G_{\rm corr}, R_s)$ for parallel circuit mode [46]:

$$G_{\rm corr} = \frac{G(1 - GR_s) - \omega^2 C^2 R_s}{(1 - GR_s)^2 + (\omega C R_s)^2}, \tag{A1}$$

$$C_{\rm corr} = C\frac{1 + G_{\rm corr} R_s}{1 - GR_s}. \tag{A2}$$

In our case, the series resistance at low temperatures is dominated by the InAlN contribution, thus depends on the length [about 200 nm $-W(V_a, T)$, where W is the depletion width] of the conducting part, which varies with temperature and applied voltage. This complicates the quantitative analysis. In any case, R_s in admittance experiments ($V_a \leqslant 0$ V) is smaller than the series resistance obtained by current-voltage measurements ($V_a > 4.5$ V). For correcting the conductance measurements on D_2 at a given temperature, we took the value of R_s [Fig. 2(b)] from the current-voltage measurements (Fig. 1). By neglecting the effect of R_s, one overestimates by 3% the activation energy.

For D_1, the situation is more delicate, since we have to know the temperature dependence of the series resistance in the range 100 K to 160 K, where the conductance peak D_1 is observed. Assuming that the power-law dependence of the mobility does not change between 100 K and 250 K, we extrapolated the lower branch shown in Fig. 2(b) to this temperature range. To get positive results for the corrected conductance, we had to apply a scaling factor to R_s. Thus, only a qualitative understanding of the effect of the series resistance $R_s(T)$ could be obtained. The series mode of measurements at 13 MHz was still dominated by the contribution of the junction part of the circuit, in most of the temperature range. Therefore, we could not simply extract $R_s(T)$ in the whole temperature range 80–400 K from measurements in the series mode.

[1] R. Butté, J.-F. Carlin, E. Feltin, M. Gonschorek, S. Nicolay, G. Christmann, D. Simeonov, A. Castiglia, J. Dorsaz, H. J. Buehlmann, S. Christopoulos, G. Baldassarri Höger von Högersthal, A. J. D. Grundy, M. Mosca, C. Pinquier, M. A. Py, F. Demangeot, J. Frandon, P. G. Lagoudakis, J. J. Baumberg, and N. Grandjean, J. Phys. D: Appl. Phys. **40**, 6328 (2007).

[2] J.-F. Carlin and M. Ilegems, Appl. Phys. Lett. **83**, 668 (2003).

[3] H. J. Kim, S. Choi, S.-S. Kim, J.-H. Ryou, P. D. Yoder, R. D. Dupuis, A. M. Fischer, K. Sun, and F. A. Ponce, Appl. Phys. Lett. **96**, 101102 (2010).

[4] F. Medjdoub, J.-F. Carlin, M. Gonschorek, E. Feltin, M. A. Py, N. Grandjean, and E. Kohn, Int. J. High Speed Electron. Syst. **17**, 91 (2007).

[5] D. Maier, M. Alomari, N. Grandjean, J.-F. Carlin, M.-A. di Forte-Poisson, C. Dua, A. Chuvilin, D. Troadec, C. Gaquière, U. Kaiser, S. L. Delage, and E. Kohn, IEEE Trans. Device Mater. Rel. **10**, 427 (2010).

[6] Y. Z. Yue, Z. Y. Hu, J. Guo, B. Sensale-Rodriguez, G. W. Li, R. H. Wang, F. Faria, T. Fang, B. Song, X. Gao, S. P. Guo, T. Kosel, G. Snider, P. Fay, D. Jena, and H. L. Xing, IEEE Electron Device Lett. **33**, 988 (2012).

[7] S. Senda, H. Jiang, and T. Egawa, Appl. Phys. Lett. **92**, 203507 (2008).

[8] A. Castiglia, E. Feltin, J. Dorsaz, G. Cosendey, J.-F. Carlin, R. Butté, and N. Grandjean, Electron. Lett. **44**, 521 (2008).

[9] Z. T. Chen, S. X. Tan, Y. Sakai, and T. Egawa, Appl. Phys. Lett. **94**, 213504 (2009).

[10] R. B. Chung, F. Wu, R. Shivaraman, S. Keller, S. P. DenBaars, J. S. Speck, and S. Nakamura, J. Cryst. Growth **324**, 163 (2011).

[11] R. B. Chung, O. Bierwagen, F. Wu, S. Keller, S. P. DenBaars, J. S. Speck, and S. Nakamura, Jpn. J. Appl. Phys. **50**, 101001 (2011).

[12] Y. Taniyasu, J.-F. Carlin, A. Castiglia, R. Butté, and N. Grandjean, Appl. Phys. Lett. **101**, 082113 (2012).

[13] C. R. Abernathy, J. D. MacKenzie, S. R. Bharatan, K. S. Jones, and S. J. Pearton, J. Vac. Sci. Technol. A **13**, 716 (1995).

[14] T.-S. Yeh, J.-M. Wu, and W.-H. Lan, J. Cryst. Growth **310**, 5308 (2008).

[15] M. J. Lukitsch, Y. V. Danylyuk, V. M. Naik, C. Huang, G. W. Auner, L. Rimai, and R. Naik, Appl. Phys. Lett. **79**, 632 (2001).

[16] P. D. C. King, T. D. Veal, A. Adikimenakis, H. Lu, L. R. Bailey, E. Iliopoulos, A. Georgakilas, W. J. Schaff, and C. F. McConville, Appl. Phys. Lett. **92**, 172105 (2008).

[17] D. J. Chadi and K. J. Chang, Phys. Rev. Lett. **61**, 873 (1988).

[18] D. J. Chadi and K. J. Chang, Phys. Rev. B **39**, 10063 (1989).

[19] T. Mattila and R. M. Nieminen, Phys. Rev. B **54**, 16676 (1996).

[20] C. G. Van de Walle, Phys. Rev. B **57**, R2033(R) (1998).

[21] M. D. McCluskey, N. M. Johnson, C. G. Van de Walle, D. P. Bour, M. Kneissl, and W. Walukiewicz, Phys. Rev. Lett. **80**, 4008 (1998).

[22] M. D. McCluskey, C. G. van de Walle, N. M. Johnson, D. P. Bour, and M. Kneissl, Int. J. Mod. Phys. B **13**, 1363 (1999).

[23] L. Gordon, J. L. Lyons, A. Janotti, and C. G. Van de Walle, Phys. Rev. B **89**, 085204 (2014).

[24] L. Silvestri, K. Dunn, S. Prawer, and F. Ladouceur, Appl. Phys. Lett. **99**, 122109 (2011).

[25] D. Johnstone, J. H. Leach, V. A. Kovalskii, Q. Fan, J. Xie, and H. Morkoç, Proc. SPIE **7216**, 72162R (2009).

[26] Z. Chen, K. Fujita, J. Ichikawa, Y. Sakai, and T. Egawa, Jpn. J. Appl. Phys. **50**, 081001 (2011).

[27] W. Chikhaoui, J.-M. Bluet, M.-A. Poisson, N. Sarazin, C. Dua, and C. Bru-Chevallier, Appl. Phys. Lett. **96**, 072107 (2010).

[28] S. Dueñas, I. Izpura, J. Arias, L. Enriquez, and J. Barbolla, J. Appl. Phys. **69**, 4300 (1991).

[29] M. P. Verkhovodov, H. P. Peka, and D. A. Pulemyotov, Semicond. Sci. Technol. **8**, 1842 (1993).

[30] G. Perillat-Merceroz, G. Cosendey, J.-F. Carlin, R. Butté, and N. Grandjean, J. Appl. Phys. **113**, 063506 (2013).

[31] T. Achtnich, G. Burri, M. A. Py, and M. Ilegems, Appl. Phys. Lett. **50**, 1730 (1987).

[32] T. Achtnich, G. Burri, and M. Ilegems, J. Vac. Sci. Technol. A **7**, 2537 (1989).

[33] L. Lugani, M. A. Py, J.-F. Carlin, and N. Grandjean, J. Appl. Phys. **115**, 074506 (2014).

[34] E. Arslan, S. Bütün, and E. Ozbay, Appl. Phys. Lett. **94**, 142106 (2009).

[35] G. Pozzovivo, J. Kuzmík, S. Golka, W. Schrenk, G. Strasser, D. Pogany, K. Čičo, M. Ťapajna, K. Fröhlich, J.-F. Carlin, M. Gonschorek, E. Feltin, and N. Grandjean, Appl. Phys. Lett. **91**, 043509 (2007).

[36] E. H. Rhoderick and R. H. Williams, *Metal-semiconductor contacts* (Clarendon Press, Oxford, 1998), Chap. 3.
[37] F. A. Padovani and R. Stratton, Solid-State Electron. **9**, 695 (1966).
[38] I. Vurgaftman and J. R. Meyer, J. Appl. Phys. **94**, 3675 (2003).
[39] H. Hasegawa and S. Oyama, J. Vac. Sci. Technol. B **20**, 1647 (2002).
[40] J. Kotani, T. Hashizume, and H. Hasegawa, J. Vac. Sci. Technol. B **22**, 2179 (2004).
[41] H. Hasegawa and M. Akazawa, J. Korean Phys. Soc. **55**, 1167 (2009).
[42] D. M. Sathaiya and S. Karmalkar, J. Appl. Phys. **99**, 093701 (2006).
[43] C. Y. Chang, Y. K. Fang, and S. M. Sze, Solid-St. Electron. **14**, 541 (1971).
[44] D. L. Losee, J. Appl. Phys. **46**, 2204 (1975).
[45] J. Barbolla, S. Dueñas, and L. Bailón, Solid-State Electron. **35**, 285 (1992).
[46] D. K. Schroder, *Semiconductor Material and Device Characterization* (Wiley, New York, 1998), Chap. 2.
[47] D. C. Look, *Electrical Characterization of GaAs Materials and Devices* (Wiley, Chichester, 1989), Chap. 4.
[48] E. Arslan, S. Bütün, S. Safak, and E. Ozbay, J. Electron. Mat. **39**, 2681 (2010).
[49] J. Frenkel, Phys. Rev. **54**, 647 (1938).
[50] S. R. Dhariwal and B. M. Deoraj, Solid-State Electron. **36**, 1165 (1993).
[51] M. Jaros, Phys. Rev. B **16**, 3694 (1977).
[52] T. L. Tansley and R. J. Egan, Phys. Rev. B **45**, 10942 (1992).
[53] I. Gorczyca, S. P. Lepkowski, T. Suski, N. E. Christensen, and A. Svane, Phys. Rev. B **80**, 075202 (2009).
[54] T. N. Theis, P. M. Mooney, and B. D. Parker, J. Electron. Mater. **20**, 35 (1991).
[55] N. Chand, T. Henderson, J. Klem, W. T. Masselink, R. Fischer, Y.-C. Chang, and H. Morkoç, Phys. Rev. B **30**, 4481 (1984).
[56] J. M. Sallese, D. K. Maude, M. L. Fille, U. Willke, P. Gibart, and J. C. Portal, Semicond. Sci. Technol. **7**, 1245 (1992).
[57] F. Rziga-Ouaja, H. Mejri, A. Triki, A. Selmi, and A. Rebey, J. Appl. Phys. **88**, 2583 (2000).
[58] A. Triki, H. Mejri, F. Rziga-Ouaja, and A. Selmi, Phys. Status Solidi B **227**, 541 (2001).
[59] S. A. Kazanskiĭ and A. I. Ryskin, Phys. Solid State **48**, 1663 (2006).
[60] E. Calleja, A. Gomez, E. Muñoz, and P. Camara, Appl. Phys. Lett. **52**, 1877 (1988).
[61] E. Calleja, F. Garcia, A. Gomez, E. Muñoz, P. M. Mooney, T. N. Morgan, and S. L. Wright, Appl. Phys. Lett. **56**, 934 (1990).